Electrical response and biodegradation of Sepia melanin-shellac films printed on paper

Check for updates

Anthony Camus [1,5], Shinhyeong Choe [2,5], Camille Bour-Cardinal [1], Joaquin Isasmendi [1], Yongjun Cho [2], Youngju Kim [2], Cristian Vlad Irimia [3], Cigdem Yumusak[3], Mihai Irimia-Vladu [3], Denis Rho [4] ✉, Jaewook Myung [2] ✉ & Clara Santato [1] ✉

Sepia melanin, a biopigment extracted from the ink sac of cuttlefish, is relevant to sustainable organic electronics. In this work, we flexographically print films from an ink of Sepia melanin including shellac as a bio-sourced binder on silver electrode-patterned paper. We examine the electrical response in high humidity and ambient conditions (here the electronic conductivity is as high as 10^{-4} S/cm). Additionally, we study the biodegradation of the printed films and their individual constituents based on their mineralization into CO_2 under composting conditions. The printed films exhibit biodegradation levels of about $97 \pm 25\%$ in 85 d. We observe microorganism colonization on the printed film's surface. The analysis of the microbial community on the compost reveals that bacterial species within the *Acidimicrobiia* class, specifically *Actinomarinales* order, are potentially responsible for the biodegradation of the printed film. Meanwhile, ecotoxicity tests conducted by germinating *Lolium multiflorum* and *Tagetes erecta* suggest that printed films have negligible phytotoxicity.

The growing demand for electronics, a highly developed and prevalent technology, intensifies the strain on critical chemical elements and leads to a dramatic accumulation of Waste of Electrical and Electronic Equipment (WEEE). This issue harbors significant geopolitical, environmental, health, and societal concerns. As of 2019, the worldwide WEEE generation was 53.6 Mt, and the fate of 82.6% of this amount (44.3 Mt) was estimated as uncertain[1]. Furthermore, electronic products exhibit a high embodied energy, primarily attributable to their complex production processes[2]. The embodied energy refers to the total energy expended throughout the entire lifecycle of a product. It includes the energy required for extracting and processing raw materials, manufacturing components, and assembling the final product.

Sustainable organic electronics proposes the use of solution-processable organic materials extracted from natural sources or synthesized following the green chemistry principles for biodegradable devices. Solution-processable (printable) materials are expected to bring about low embodied-energy electronics since processing takes place at ambient conditions (i.e., no high vacuum or high temperature conditions are employed).

Eumelanin, the black-brown natural pigment member of the melanin family, has been investigated to explore the potential of sustainable organic electronics[3]. Sepia melanin is a form of eumelanin that can be extracted from cuttlefish ink (Sepia officinalis)[4]. Sepia melanin is composed of nanometric granules (100–200 nm in diameter) that result from the hierarchical development of oligomers of its building blocks (monomers), namely 5,6-dihydroxyindole and 5,6-dihydroxyindole-2-carboxylic acid (respectively DHI and DHICA, Table 1)[5–7]. The electronic conjugation of the DHI and DHICA building blocks opens the possibility to observe electronic transport in the eumelanin macromolecule[8–12]. The transport physics of eumelanin has been the subject of intensive studies, in the past decades. In the 1970s, McGinness et al. explained the electrical resistive switching observed in pellets of hydrated eumelanin through the amorphous semiconductor model[13]. Mostert et al. by observing the effect of the hydration degree on the electrical conductivity of synthetic eumelanin, proposed a mixed protonic-electronic conduction model[14–16]. Recently, Reali et al. investigated natural Sepia melanin, observing predominant electronic transport in dry pellets of the biopigment[12].

We recently reported on an electronic conductivity as high as 10^{-3} S/cm in films deposited on Au-patterned SiO_2 substrates from an ink of Sepia melanin and the synthetic polyvinyl butyral (PVB) binder[17]. The conductivity was attributed to inter-granule percolation paths, generated by the confining action of the PVB binder. Films made from ink formulation

[1]Engineering Physics Department, Polytechnique Montréal, 2900 Édouard Montpetit, Québec, QC, Canada. [2]Department of Civil and Environmental Engineering, KAIST, Daejeon, Republic of Korea. [3]Linz Institute for Organic Solar Cells (LIOS), Institute of Physical Chemistry, Johannes Kepler University Linz, Altenberger Str. Nr. 69, Linz, Austria. [4]Consultant Biotech, Montreal, Canada (retiree NRC Researcher), Montreal, QC, Canada. [5]These authors contributed equally: Anthony Camus, Shinhyeong Choe. ✉e-mail: rho.denis29@gmail.com; jjaimyung@kaist.ac.kr; clara.santato@polymtl.ca

including the PVB binder were not responsive to environmental moisture because the hydrophobic binder protects the Sepia melanin granules. Besides extraction from Sepia ink, Eumelanin can be obtained from food industry waste (See Insectta ®) and biotechnological routes[18,19].

Bio-sourced binders, such as shellac, are attractive for sustainable electronics. Shellac is a natural resin, secreted by insects from the Kerria lacca family, a lac insect[20,21]. It has been used in several applications due to its film-forming properties, thermo-plasticity, hydrophobicity, and high solubility in alkali solvents. Shellac has been recently used as a mechanical substrate and dielectric material in organic transistors[22,23], and as a binder in printed carbon-loaded ink[24].

Given the potential environmental impact of electronic devices and the risk of eco-toxicity if materials are not properly managed at the end of their life cycle, the investigation of compostability becomes particularly relevant.

Composting is a common practice for organic waste management, adopted by municipalities around the world[25]. It is a biochemical process in which organic waste is transformed into CO_2, water, biomass, and eventually becomes a nutrient-rich humic compost that can enhance soil fertility. During composting, organic materials are exposed to conditions favorable for rapid degradation, including thermophilic conditions, 50–60 °C, adequate water content (50–60 wt%), and an abundant and diverse population of microorganisms, with counts ranging between 10^7 and 10^8 colony-forming units per gram of compost[25–27].

The biodegradation of organic materials can be followed by the mineralization of organic carbon into CO_2[26,28–31]. Upon its biodegradation, an organic material should not leave behind harmful residual substances that could impair the quality of the final compost, which is commonly used as fertilizer.

In this work, a cradle-to-grave study is presented for films made from bio-sourced materials (Sepia melanin extracted from natural cuttlefish ink and shellac) deposited using a low embodied energy approach, specifically flexographic printing on silver-patterned paper. Initially, we characterized the morphology of the films using scanning electron microscopy (SEM), and their electrical response was evaluated in ambient and wet environmental conditions through current-voltage (I-V), current-time (I-t), and impedance spectroscopy (IS). Subsequently, we explored the biological degradation of the printed films using respirometry, metagenomic, and ecotoxicity analyses. The respirometry method requires only a small quantity of active compost and few grams of test material to assess its biodegradation under composting conditions.

Results and Discussion

### Shellac as a dielectric material for blended inks

We initially assessed the properties of biosourced shellac to determine its effectiveness as a binder in ink formulations containing conductive Sepia melanin granules. Shellac films were deposited onto glass substrates fitted with two parallel aluminum (top) and gold (bottom) electrodes, each 1 mm wide and 80 nm thick. These electrodes were applied using a physical vapor deposition system. The shellac solution was prepared in pure ethanol, and the films were created using a fabrication method detailed in Materials and Methods. After drying the spin-coated shellac film, we completed the metal-insulator-metal (MIM) structure, namely aluminum-shellac-gold, by depositing two additional parallel aluminum electrodes. These top electrodes, each 80 nm thick and 1 mm wide, were deposited at a 90° angle to the bottom electrodes using the same physical vapor deposition system. We fabricated 12 MIM samples in total, creating 3 glass slides with 4 MIM structures on each. These samples showed excellent reproducibility, with negligible impedance measurement variation. A typical dielectric investigation is displayed in Fig. 1a.

Shellac is a robust dielectric material[22]. De-waxed shellac films demonstrated robust dielectric properties, evidenced by a uniform dielectric constant measured over 7 orders of magnitude frequency (i.e. 10 kHz to 1 mHz, black line in Fig. 1a). The loss angle (i.e. the ratio ε"/ε', imaginary and real part of the dielectric constant, respectively), did not show any relaxation and remained below 0.1, even at 1 mHz. This behavior is characteristic of an exceptionally pure dielectric material[22,32–34].

The calculated dielectric constant of shellac was, 4.05 ± 0.2 resulted from the measurement of the capacitances and thicknesses of the 12 samples involved in the impedance measurement. The measured breakdown field of the shellac films (following the experimental conditions described in Materials and methods) varied with sample thickness[35]. At the two extremes, we measured an average breakdown field of ~2.1 MV/cm for a ~2000 nm thick set of samples, and ~8 MV/cm for a set of thinner samples of ~400 nm (Supplementary Fig. 1). Fig. 1b shows the breakdown field behavior (capacitance as function of the applied bias) of a sample of 2100 nm shellac thick film with a breakdown field of 2.1 MV/cm.

### Morphology and electrical response of printed films

Sepia melanin-shellac printed films exhibit a distinctive nanostructured morphology, with Shellac embedding Sepia melanin nanogranules (Fig. 2). The enhanced contact between granules of Sepia melanin can lead to the formation of continuous paths for the percolation of charge carriers[17].

a)

b)
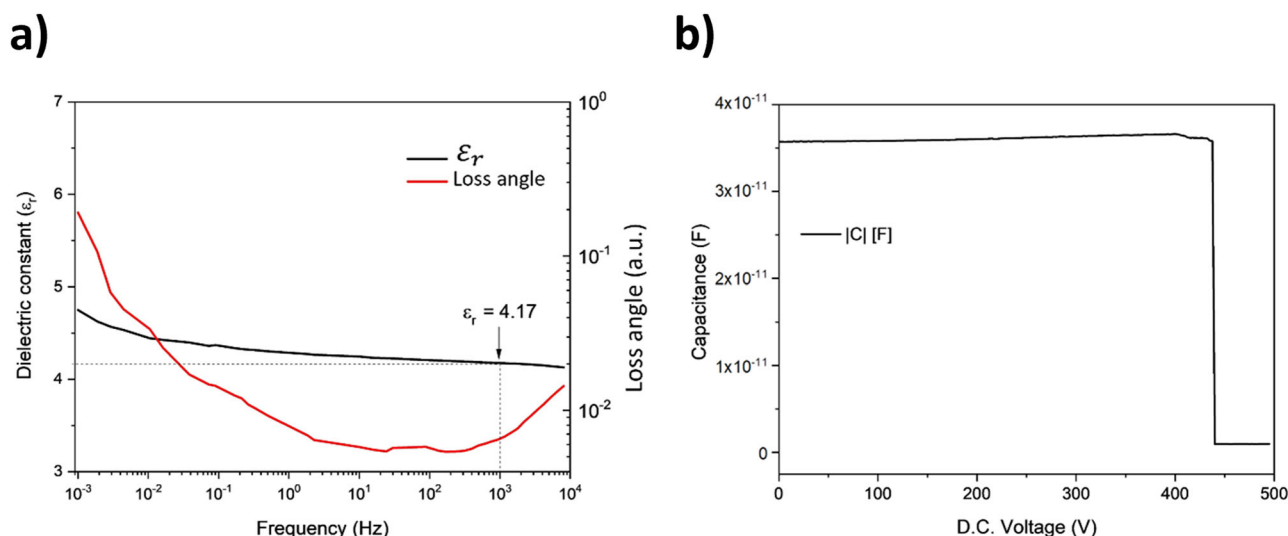
Fig. 1 | Dielectric investigation of pure dewaxed shellac films. a Dielectric spectroscopy (dielectric constant and loss angle) of dewaxed shellac in a wide frequency range, spanning from 10 kHz to 1 mHz; **b** Breakdown field measurement of shellac films (2 V increment, 5 s hold time at each measurement point). The electrodes in the MIM configuration were Au as bottom electrode and Al as top electrode.

Fig. 2 | SEM images of Sepia melanin-shellac printed films on Ag electrode-patterned paper. **a** topography and **b** metallized cross-section. Inset in **a** is an optical image of printed film on Ag electrode-patterned paper.
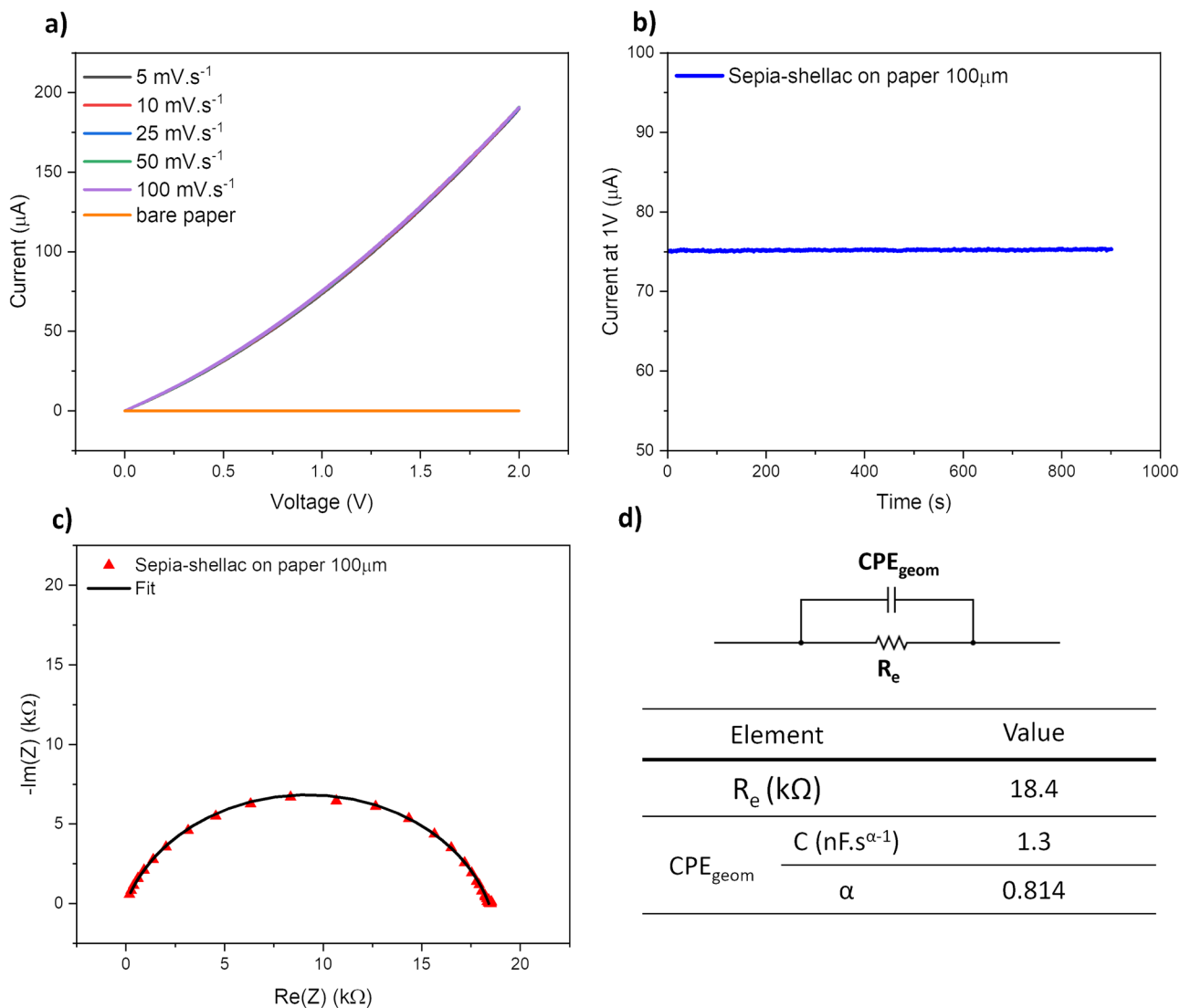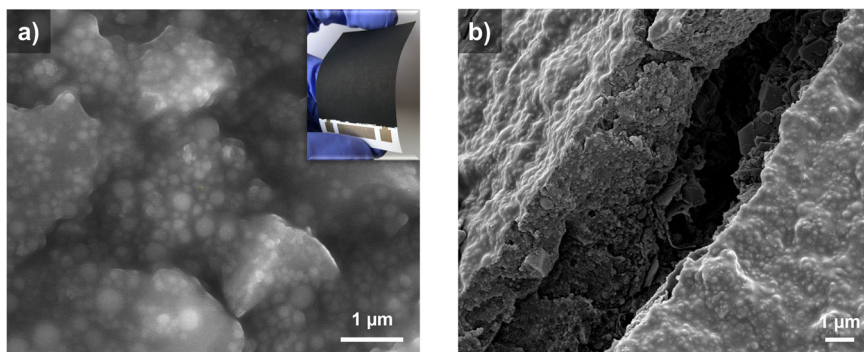
Fig. 3 | Electrical and electrochemical characterization of Sepia melanin-shellac printed film on silver-electrode patterned paper, in ambient conditions. **a** Current-voltage response as a function of the potential scan rate. The response of the bare paper substrate is included. **b** Transient current at 1 V. **c** Nyquist plot from impedance spectroscopy (IS). **d** Equivalent circuit model used to fit the Nyquist plot and a table with the extracted values; R_e is the film resistance and CPE_{geom} is the constant phase element representing the geometrical capacitance of the system. α is a dimensionless number comprised between 0 and 1 that quantifies how close the element is to a pure capacitor ($\alpha = 1$).

We evaluated the current-voltage (I-V) characteristics of these films on silver-electrode patterned paper substrates under ambient conditions (20 °C, 30% RH), as depicted in Fig. 3a. The current increases with the voltage (conductivity of about 10^{-4} S/cm at 2 V). The current does not depend on the potential scan rate and no hysteresis is observable. These findings strongly indicate that the contribution of ionic transport to the electrical response is negligible. The current-time (I-t) characteristics show a plateau-like behavior; no exponential decay of the current attributable to the

formation of an ionic double layer is observable (Fig. 3b). Impedance spectroscopy (IS) measurements were performed to measure the impedance of the printed film over a wide range of applied frequencies. The measurements revealed the presence of a single semi-circle in the Nyquist plot (i.e., negative imaginary part of the impedance, -Im(Z), as function of the real part of the impedance, Re(Z), (Fig. 3c). This specific characteristic can be represented by a Resistance-Capacitance (RC) equivalent circuit (Fig. 3d). The geometrical capacitance (CPE_{geom}) is fundamentally related to the film dielectric properties, i.e., to store electrical charges between the metallic electrodes. This type of equivalent circuit is in agreement with the presence of only one type of charge carrier (in the present case, electronic) in the films[36]. I-V, I-t, and IS measurements point towards predominant electronic transport in printed films of Sepia melanin-shellac, in ambient conditions.

Hydration-dependent electrical characteristics

Eumelanin is recognized to feature an electrical response dependent on its hydration level[12,16,37]. Owing to the observed predominance of electronic charge carriers in the film in dry conditions (20 °C, 30% RH), we probed the

potential transition of the current from electronic to mixed ionic-electronic by examining the electrical response of Sepia melanin-shellac printed films in a wet atmosphere (20 °C, 85% RH).

Following 24 hr at 85% RH, which resulted in approximately 14 wt% moisture absorption, the current values notably increased compared to ambient conditions, as shown in Fig. 4a. In the Nyquist plots, hydrated samples display two semi-circles, indicative of parallel electronic and ionic contributions (Fig. 4c, d). The first semi-circle, at high frequencies, can be modelled by an ionic resistance, R_i, and geometrical capacitance, CPE_{geom}, in parallel (Fig. 4c). On the other hand, the second semi-circle at lower frequencies can be modelled by electronic resistance, R_e, and geometrical capacitance, CPE_{geom}, in parallel[36]. The extraction of resistances from fits based on equivalent circuit models (Fig. 4d, Supplementary Fig. 2) reveals that the electronic resistance does not significantly change with relative humidity (R_e is about 18 kΩ before and about 22 kΩ after hydration). The ionic resistance, R_i, can be estimated at about 88 kΩ (Supplementary Fig. 2). The increase of CPE_{geom} upon hydration (Supplementary Fig. 2) is due to the absorption of moisture by the system (here, mainly the paper).
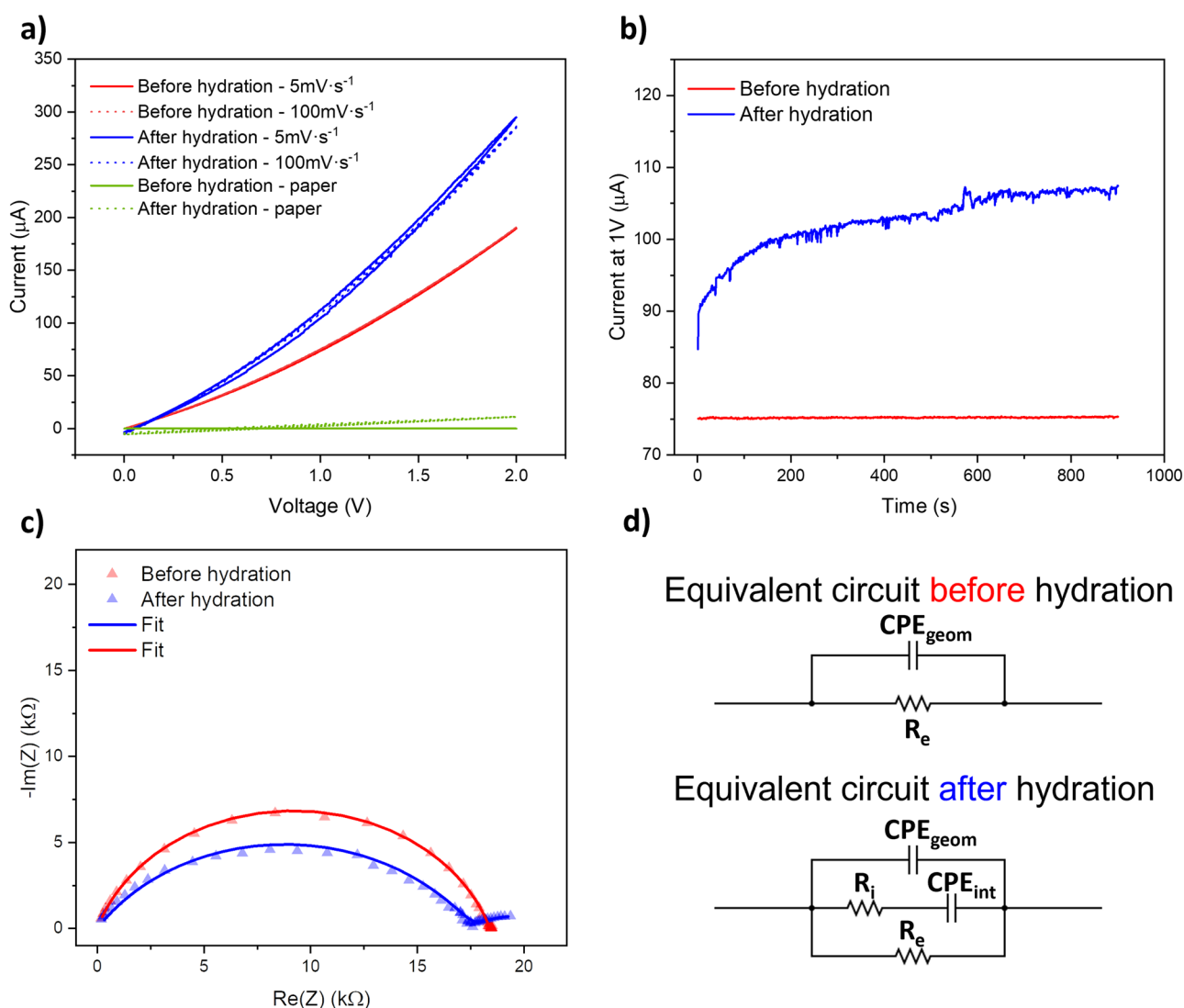
Fig. 4 | Hydration-dependent electrical response of Sepia melanin-shellac printed film on silver patterned paper. Red and blue curves are respectively the electrical responses of the samples before and after hydration at 85% RH, during 24 hr. **a** Current-voltage response for two scan rates of the electrical potential. Bare paper current-voltage response at 100 mV·s⁻¹ was included for reference. **b** Transient current at 1 V. **c** Nyquist plot from IS. **d** Equivalent circuit used to fit the Nyquist plots. R_e and R_i are the film resistances for electronic and ionic respectively. The CPE_{int} represents the interfacial capacitance, which describes the capacitive properties of the film/metal electrode interfaces. On the other hand, CPE_{geom} is the geometrical capacitance, and describes the dielectric constant of the material between two metallic contacts[36].

Water being a high dielectric constant liquid, the capacitance of the system increases.

The bare Kromekote® paper substrate shows a significant electrical response when hydrated (Supplementary Fig. 3). The hydrated paper features ionic conduction (with ionic resistance in the order of 100 kΩ), namely, a diffusion tail at low frequencies in the Nyquist plot from IS, exponential decay in the transient current, and hysteresis in the current-voltage responses (Supplementary Fig. 3).

After hydration, the current-time characteristics of Sepia melanin-shellac printed film on paper obtained at 1 V, show two regions (blue curve, Fig. 4b). In the former region, we observe a current increase from about 85 to 100 μA (in about 200 s); in the latter region, a quasi-plateau behavior. We make the hypothesis that, in the former region, the shape of the current results from several factors, such as the decrease of the injection barrier with the formation of electrical (ionic) double layers (EDL) at the film/metal interfaces (also responsible of a non-significant decay)[38] and local effective doping by field ionization and/or ion redistribution[39].

Owing to the hydrophobicity of Shellac and the absorption of moisture by paper, we make the hypothesis that ionic (protonic) conduction of the samples mainly occurs through the paper. The similarity of values of ionic resistances of hydrated paper and hydrated Sepia-shellac printed film together with the absence of a third semi-circle in the Nyquist plot attributable to granule boundaries-induced capacitance, support such hypothesis[36]. Thus, we think that shellac is acting as a protective (hydrophobic) matrix, limiting the hydration of the Sepia melanin granules actively participating in the percolative conduction of the system.

Thermal treatment: cross-linking

Shellac's thermal and mechanical properties make it an appealing choice for a binder in ink formulations. Sepia melanin-shellac printed film thermally treated at 70 °C for 1 hr shows a significant increase in electrical conductivity (Supplementary Fig. 4). We hypothesize that by heating the printed film close to its melting temperature (75 °C), the shellac matrix can soften, opening the opportunity for the Sepia melanin granules to rearrange and enhance their mutual contact. Moreover, heating at 70 °C could increase the shellac cross-linking degree (mechanical stability) by polyesterification of

molecular components and weak physical interactions (van der Waals and H-bonding)[22,24,40].

Biodegradation test under controlled composting conditions

The biodegradation test aims at investigating the potential end-of-life scenario for Sepia melanin-shellac printed films and their constituents, including Sepia melanin, shellac, and cellulose. The biodegradation test was conducted in a laboratory setting, replicating controlled composting, including thermophilic conditions at 58 °C, a water content range of 50–60%, and aeration rate of 80–100 mL min^{-1}. The respiration activity of the compost microbiota was continuously monitored using a lab-scale respirometer over 85 d (Fig. 5 and Table 1).

The microcrystalline α-cellulose (powder) showed a level of biodegradation of 87 ± 13% over 85 d. The mineralization level of cellulose closely corresponded to our prior findings (83% in 38 d)[41,42]. Sepia melanin (powder) showed 33 ± 19% mineralization in 85 d, slightly lower than our previous study (37% in 98 d)[42]. The observed differences in the biodegradation level of Sepia melanin are primarily attributed to the following factors: (i) the specific type of organic material from which the compost was prepared, whether lignocellulosic biomass[42] or manure (this work) and (ii) the experimental configuration and (iii) the composition of the microbiota[42]. These factors could also explain the large standard deviations (cumulatively computed) of the respirometry results.

Shellac (flakes) exhibited 12 ± 7% mineralization in 85 d. It was previously reported that pure shellac shows 11.3% weight loss in garden soil after 30 d[31,43]. The limited biodegradation of shellac can be explained by its chemical structure and hydrophobicity. The hydrophobicity of shellac may reduce the number of water molecules on the surface, thus limiting hydrolytic breakdown that governs the biodegradation rate of polymer materials[29]. Moreover, shellac is mainly composed of aleuritic acids and cyclic terpene acids linked by ester bonds[21]. While ester bonds can undergo hydrolytic cleavage when exposed to water and high temperatures (e.g., 58 °C), the resulting oligomers and monomers might remain relatively inaccessible to the compost microbiota leading to reduced biodegradation, i.e., low mineralization.

The printed film displayed a significant biodegradation level of 97 ± 25% in 85 d. Remarkably, despite being composed of 95 wt% silver electrode-
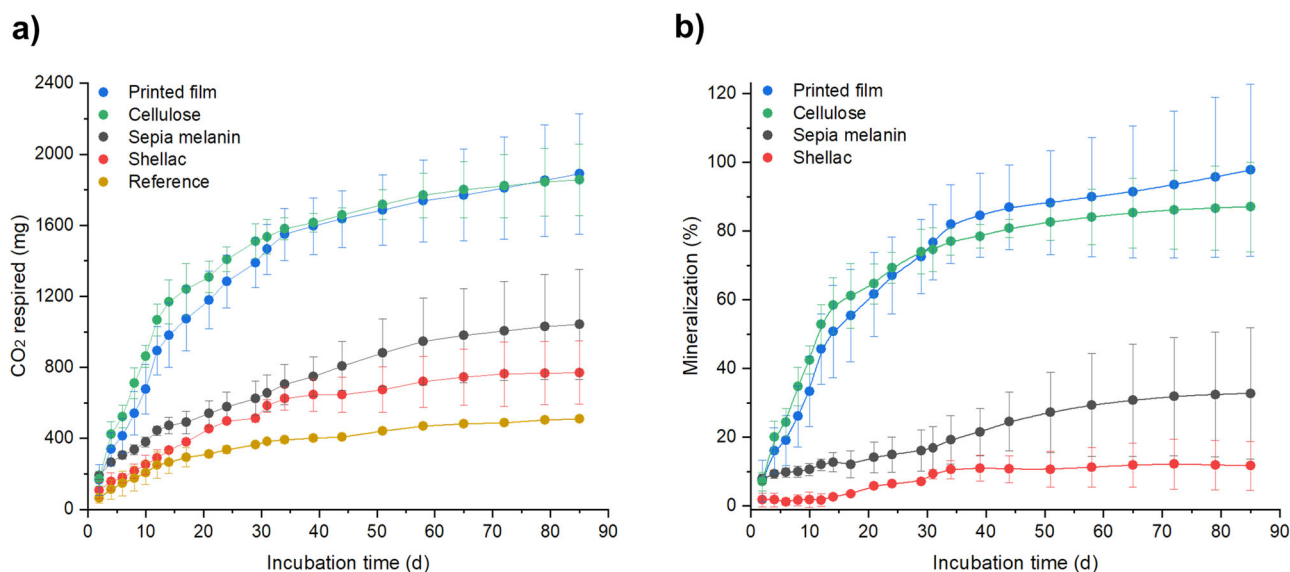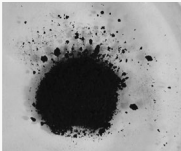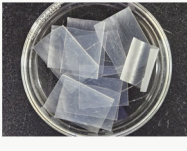
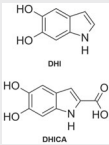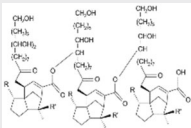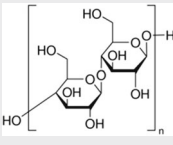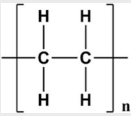**Fig. 5 | Biodegradation test results of Sepia melanin-shellac printed film on silver-electrode patterned paper and its constituents under composting conditions.** a Cumulative CO$_2$ respired. b Mineralization levels of Sepia melanin, shellac, printed film, and cellulose under controlled composting conditions (58 °C, 50–60% RH), calculated as the difference of the CO$_2$ respired between compost containing test materials as organic substrates and reference compost, and divided by theoretical CO$_2$ production from biodegradation. The reference compost indicates the compost-only bioreactor, without any added ingredient. Error bars indicate standard deviations of cumulative values ($n = 3$ for printed film and cellulose, $n = 2$ for Sepia melanin, shellac, and reference). LDPE results are presented in Supplementary Fig. 5.

Table 1 | Summary of biodegradation test results

	Sepia melanin	Shellac	α-Cellulose	Printed film	LDPE
Sample					
Chemical structure				*	
Format	Powder	Flake	Powder	Multi-layer film	Sheet
Carbon content (wt%)	63.3	67.3	42.0	35.8	84.8
Average sample weight (mg)	701	1011	1005	1077	1012
Theoretical respired CO_2 (mg)	1625	2495	1547	1414	3149
Net respired CO_2 (mg) At 29 d At 85 d	261 ± 98 531 ± 310	177 ± 21 290 ± 178	1144 ± 100 1346 ± 202	1024 ± 140 1378 ± 340	335 ± 95 728 ± 282
Mineralization (%) 85 d	33 ± 19	12 ± 7	87 ± 13	97 ± 25	**
Half-life (d)	119.5	344.8	15.3	14.8	**

The values of net CO_2 (mg) at 29 d and 85 d, as well as mineralization levels (%), represent the average of biological replicates ($n = 3$ for printed film and cellulose, $n = 2$ for Sepia melanin, shellac, and reference). The half-life of samples is estimated based on the first-order decay model (see supporting information). *The printed film comprises Kromekote® paper (94 wt%), Ag-based electrodes (1 wt%), and a film composed of Sepia melanin and shellac (5 wt%). **LDPE results are presented in Supplementary Fig. 5.
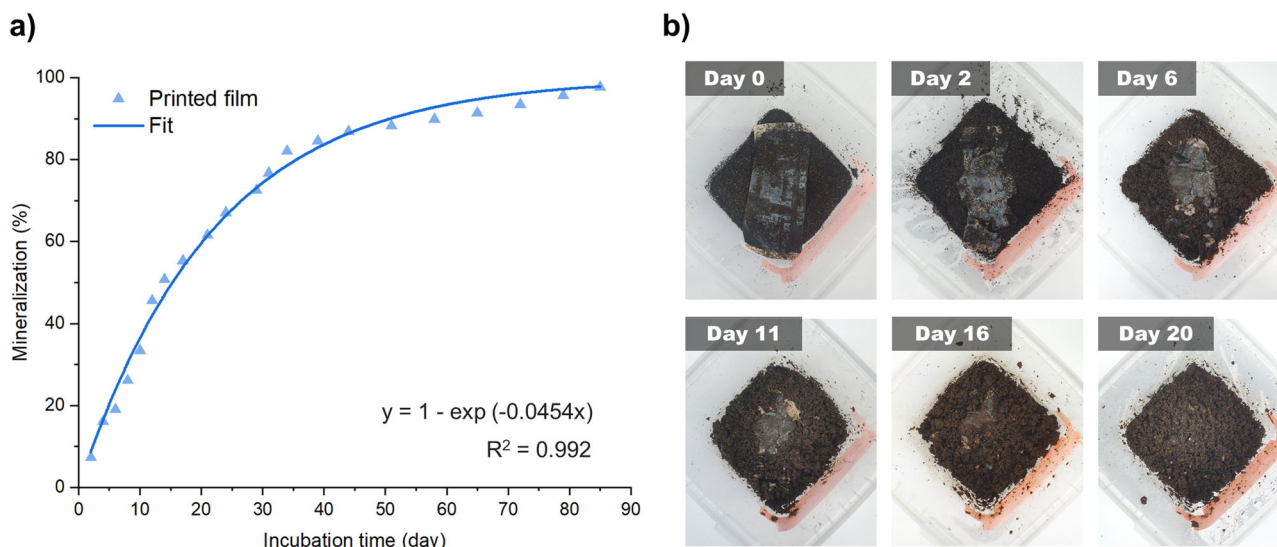

Fig. 6 | Mineralization curve of the printed film, fitted by the first-order decay kinetic model, and its rapid disintegration under composting conditions. **a** Mineralization (%) calculated from the cumulative net respired CO_2 data of the printed film fitted by the first-order kinetic model under controlled composting biodegradation testing conditions (half-life = 14.8 d). **b** Time-lapse photos of a microcosm experiment displaying the rapid disintegration of the printed film in 20 d.

patterned paper substrate and 5 wt% of Sepia melanin-shellac printed layer, the printed film's average mineralization level exceeded that of microcrystalline α-cellulose from 30 d of incubation. This suggests that the presence of Sepia melanin-shellac and silver electrodes (in this specific configuration) did not impede the biodegradation process of the printed film. We hypothesize that the hygroscopic nature of the paper substrate allows for water absorption, facilitating the enzymatic hydrolysis of the core structure of the

multilayer printed film, even with the presence of silver electrodes and Sepia melanin granules embedded in a hydrophobic shellac matrix.

The mineralization curve of the printed film closely follows the first-order decay model ($R^2 = 0.992$, $p < 0.001$), and it is projected to reach 99.9% mineralization at 153 d (Fig. 6a).

We carried out microcosm experiment to assess the degradation rate of printed film and observe the microorganisms involved in the degradation
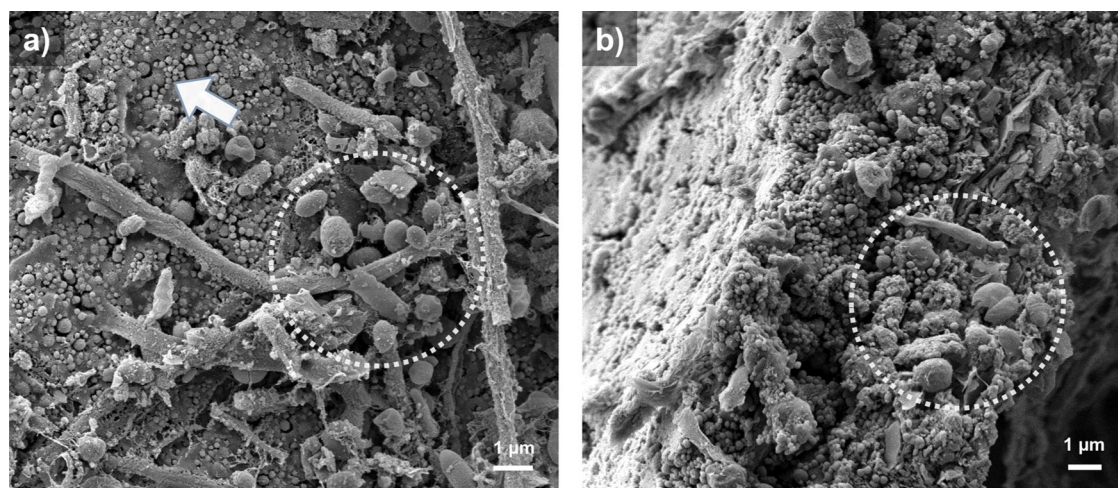
Fig. 7 | SEM images capturing an area from the printed films recovered after 13 days of incubation under composting conditions. a topography and **b** cross-sectional view. The arrow points to the Sepia melanin nanostructures, whereas the dotted circles indicate the colonization by microbial cells, of the surface, in **a** and, in **b** cross-section. The dotted line in **b** indicates the top surface of the printed film.
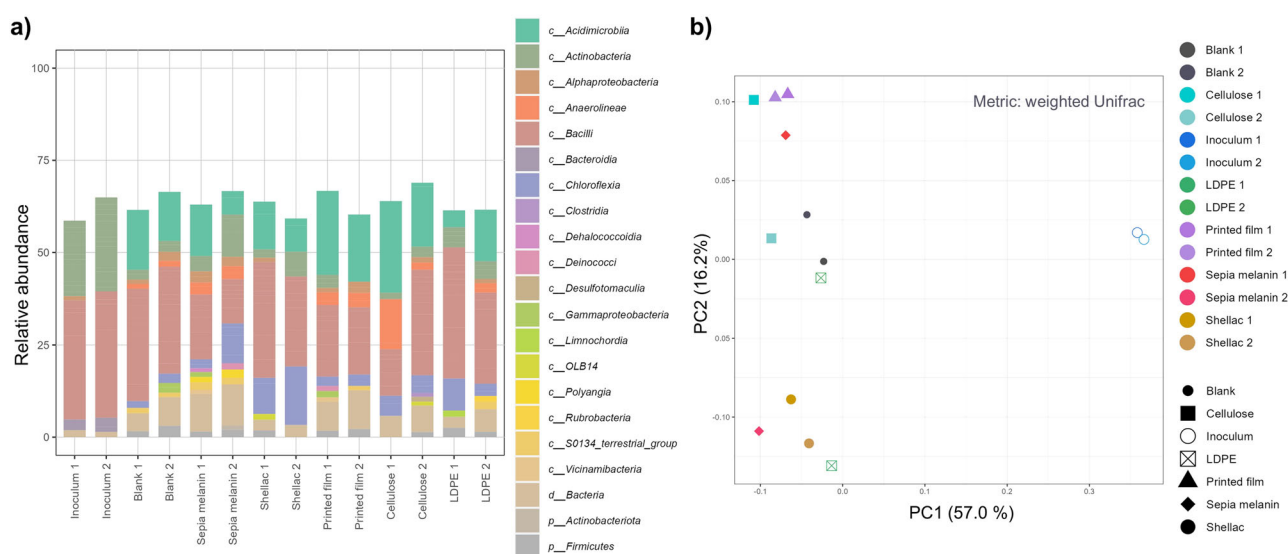
Fig. 8 | Microbial community analysis in compost after 85 days of the biodegradation test. a Class-level bacterial taxonomic affiliations and relative abundance of the 16s rRNA gene sequences representing > 1.0% of the amplicon sequence variants as the best BLAST hit, i.e., the closest taxon. **b** Principal coordinate analysis (PCoA) based on the weighted Unifrac distance of the compost microbial community at times 0 and 85 d in thermophilic composting conditions. Inoculum denotes the compost before the start of the biodegradation test and reference represents compost incubated without test material.

using the same compost (Fig. 6b, Supplementary Fig. 6), the printed films exhibited rapid degradation behavior, with complete visual disintegration was observed in approximately 20 d. The colonization of the Sepia melanin-shellac printed film by diverse microorganisms was observed after 13 days of incubation using a Scanning Electron Microscope (SEM) (Fig. 7, Supplementary Fig. 7). These images and, other SEM images in SI, confirm the presence of numerous microbial cells with varying sizes and morphologies. The majority are spherical (*cocci*), some are rod-shaped (*coccobacilli*), and a few exhibits mycelium-like *hyphae* (Fig. 7a). The cross-section image (Fig. 7b) also shows signs of colonization by some microorganisms, indicating that the structures of the printed film are compromised due to the formation of a biofilm. These observations, along with signs of structural heterogeneity, suggest a gradual breakdown and biodegradation of the film and its constituents in compost conditions. This observation aligns with prior studies that reported biofilm formation on polymer materials, including biodegradable poly(butylene adipate-*co*-terephthalate) polyester

in soil[30,44]. Furthermore, cross-sectional micrographs of the printed films confirmed the depth-wise degradation and microbial colonization (Fig. 7b). Interestingly, the spherical structures smaller than 1 μm (i.e., nanometer-sized) in diameter are not microorganisms but are most likely Sepia melanin granules[11].

Compost microbial community after biodegradation test

The microbiome of compost collected at time 0 (i.e., inoculum) and at the end of the biodegradation test (85 d) was analyzed through 16 S rRNA gene amplicon sequencing. The analysis unveiled the presence of over 400 operational taxonomic units (OTUs), collectively representing the bacterial community. We conducted relative abundance analysis at various taxonomic levels, including phylum, class, and genus (Fig. 8a, Supplementary Figs. 8, 9).

The Shannon index, which indicates biodiversity by considering both species richness and evenness, measured 7.5 for the inoculum and 8.2 for the reference compost on 85 d (Supplementary Table 1). Following the
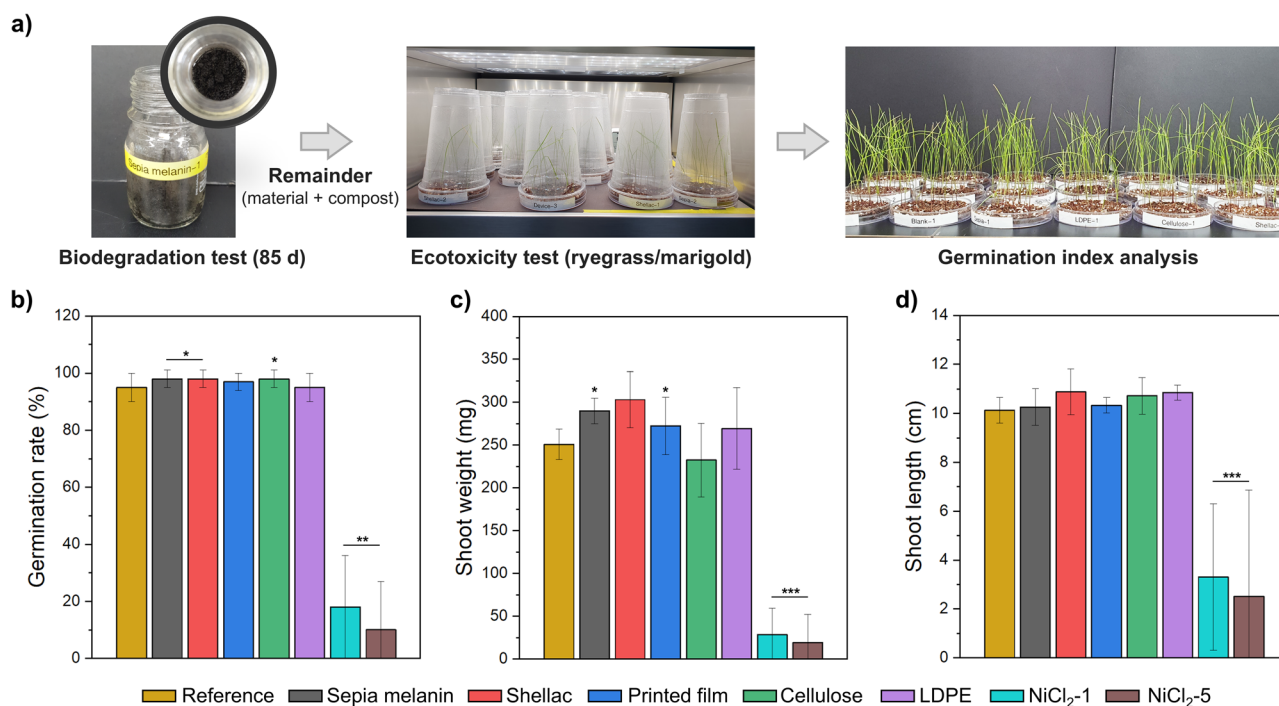
Fig. 9 | Ecotoxicity test results using ryegrass (*Lolium multiflorum*) seeds.
a Experimental process. **b** Germination rate. **c** Shoot biomass wet weight. **d** Shoot length.
The Student's t-test was used to examine statistically significant differences between the
means (*$p < 0.05$, **$p < 0.01$, ***$p < 0.001$). Error bars indicate standard deviations
($n = 3$). Marigold results are presented in Supplementary Fig. 12.

completion of the test, the Shannon index for each bioreactor remained within this range, despite the introduction of exogenous organic carbon sources, such as Sepia melanin (8.0), shellac (7.9), printed films (7.8), cellulose (7.6), and LDPE (8.0). This suggests that the prevalent two phyla in the inoculum (i.e., initial compost): *Bacillota* (formerly *Firmicutes*, 43.4%) and *Actinobacteriota* (30.6%) are closely related to organic compound degradation.

Principal coordinates analysis (PCoA) was performed based on a weighted UniFrac matrix and revealed that the shift in the microbial community was dictated by the physicochemical properties of the test materials (Fig. 7b). Sepia melanin 1, featuring moderate biodegradation, exhibited a microbial community similar to that of printed film. In contrast, Sepia melanin 2, with a low biodegradation level, resembled the microbial community of shellac. These variations likely contributed to the high standard deviation in the biodegradation levels observed for Sepia melanin (33 ± 19%) on 85 d.

Acidimicrobiia, which constituted 0.9% of the inoculum community, proliferated during the biodegradation test: reference compost (16.5%), Sepia melanin (12.8%), shellac (12.0%), printed films (22.6%), cellulose (23.3%), and LDPE (10.4%). The relative abundance of *Acidimicrobiia* exhibits a positive correlation with the mineralization level of test materials ($R = 0.906$, $n = 5$, Supplementary Fig. 10), indicating their involvement in the degradation process. This indicates that the bacterial species in the class *Acidimicrobiia* may have metabolized the test materials as new carbon and energy sources, outcompeting other microorganisms.

The initial pH of the compost was 8.6, with a final pH range which varied from 7.7 to 9.0. These variations corresponded with minor alterations in the microbial community structure for all the tested materials. The *Acidimicrobiia* class, though less extensively studied, exhibited tolerance for pH levels exceeding 7.0. We propose that species within the *Acidimicrobiia* class, specifically *Actinomarinales* (order), play a pivotal role in cellulose degradation. This hypothesis is supported by the comparison of relative abundance in cellulose-rich materials such as printed films (20.8%) and cellulose (20.8%) in contrast to cellulose-lacking materials like Sepia melanin (8.8%), shellac (8.4%), and LDPE (9.4%). Notably, a similar shift in

microbial community structure was observed between the inoculum (0.6%) and the reference compost (15.0%). The species in class *Acidimicrobiia* have previously been associated with compost maturation[45], hydrocarbon degradation in oil-contaminated environments[46], and the breakdown of complex polymers[47].

Phytotoxicity test using plant models
Given that municipalities provide compost to their residents, it is paramount to assess the environmental impact of newly claimed compostable organic waste products, ensuring no visible or toxic residues are left behind after the composting process. To evaluate the effect of the printed film and its components on flora, a laboratory-based ecotoxicity test was conducted. This assessment involved the germination testing of ryegrass (*Lolium multiflorum*) and marigold (*Tagetes erecta*) seeds. The concentration of added materials used in the biodegradation test varied within the range of 1.65% to 2.36%. Nickel chloride ($NiCl_2$) was introduced at concentrations of 1% and 5% by weight as positive control.

Lolium multiflorum (ryegrass) seeds were planted in the soil alongside compost collected after 85 d of incubation (Fig. 9a). After 14 d of incubation, *Lolium multiflorum* exhibited robust growth in the compost samples, which included Sepia melanin, shellac, printed film, cellulose, and reference compost (Supplementary Table 2).

As expected, the introduction of $NiCl_2$ to the reference compost resulted in a low germination rate and significant phenotypic damage, characterized by stunted growth, morphological alterations, and discoloration (Supplementary Figs. 11, 12). The seed emergence rates for the four tested materials, ranging from 95% to 98%, were comparable to those observed in the reference compost (95 ± 5%) (Fig. 9a). In stark contrast, the presence of $NiCl_2$ led to significantly lower seed germination rates, ranging from 10% to 18%.

The wet weight and length of the shoot, collected after 14 d of germination and growth, exhibited minimal variations among the different samples: Sepia melanin (290.1 mg), shellac (303.1 mg), printed film (272.4 mg), cellulose (232.5 mg), reference compost (250.8 mg), $NiCl_2$-1 (28.5 mg), and $NiCl_2$-5 (19.1 mg) (Fig. 8b). The shoot length of the reference compost averaged 10.1 ± 0.5 cm. The printed film displayed a similar

average shoot length (10.3 ± 0.3 cm), while NiCl$_2$-1 and NiCl$_2$-5 resulted in shoot lengths of 2.5 cm and 3.3 cm, respectively (Fig. 9c).

The tested plant models represent monocot (ryegrass) and dicot (marigold), respectively (Supplementary Figs. 11, 12). We performed a second ecotoxicity test using dicot plants such as marigold (*Tagetes erecta*) to investigate the ecotoxicity of composts to the dicot plant. These seeds were exposed to a sample of compost collected from the printed film on 85 d (Supplementary Fig. 11, 12). After 14 d of incubation, the Marigold seeds exhibited vigorous growth without any observable signs of phenotypic damage.

Conclusion

We report on a holistic study of bio-sourced materials used in ink formulations to flexographically print films for biodegradable organic electronics. The work includes a carefully considered choice of materials, the electrical characterization of the films printed on silver-patterned paper, and their biodegradation in compost conditions, including metagenomic analysis and eco-toxicity tests. The ink includes Sepia melanin as the electronic material and shellac as the binder. SEM reveals the intimate contact between the Sepia melanin granules, bringing about percolative inter-granular paths for electronic conduction. Under hydrated conditions, the electrical response indicates that the hydrophobic shellac binder protects the conductive paths within Sepia melanin from moisture. Nevertheless, the paper substrate absorbs humidity and acts as a source of protons in the system. The introduction of ionic charge carriers seems to influence the electronic conductivity by i) decreasing the barrier for the injection of electronic charge carriers with the formation of electrical (ionic) double layers at the film/metal interface and/or by ii) local effective doping by field ionization and/or ion redistribution. Sepia melanin-shellac printed films can be thermally treated at 70 °C for 1 hr to increase the system conductivity by a factor of about 2.

To the best of our knowledge, for the first time, we explored the composting of electronic materials and printed films in small bioreactors, suitable to study such class of materials, usually featuring high chemical purity and cost. The printed film (Sepia melanin-shellac on silver-electrode patterned paper) can be significantly mineralized into CO$_2$ in composting conditions (97 ± 25 % in 85 d). The microcosm (visual) experiment confirms the rapid biodegradation of the printed films in just 20 d. Diverse microorganisms' surface colonization, as observed with SEM, supports biodegradation of printed film by the compost microbiota. The observed shift in the microbial community within the compost, following the biodegradation tests, indicates that bacterial species belonging to the *Acidimicrobiia* class, specifically within the Actinomarinales order, are likely key contributors to the degradation of the printed films. Ecotoxicity tests involving the germination of *Lolium multiflorum* and *Tagetes erecta* also demonstrate that the printed films and their constituents do not cause phytotoxicity. In perspective, we plan to engineer the microbiota to improve the efficiency of the composting process. We aim to expand biodegradation research, exploring diverse bio-sourced materials under composting conditions. Key factors include microbial community structures, enzyme functions, film wettability, oxygen mass transfer, and optimal particle size for composting kinetics. Future studies should focus on real-world composting facilities, considering public and regulatory acceptability. Accurate evaluation of the environmental impact, including the embodied energy and CO$_2$ footprint, is often neglected in the scientific literature but is essential for measuring the sustainability aspect of electronic materials and devices. Work is in progress to quantify the environmental footprint of extracting Sepia melanin from cuttlefish ink using life-cycle assessment tools. This effort represents a crucial step toward establishing metrics for organic electronic materials originating from natural sources. Results reported in this work constitute the foundation for biodegradation studies presently ongoing on electrochemical energy storage devices (supercapacitors) and solar energy conversion devices based on Sepia melanin. In conclusion, these findings affirm the significant potential of using biosourced materials and paper substrates in the development of biodegradable electronic technologies, marking a

significant stride towards the realization of environmentally benign organic electronics.

Methods
Chemicals

α-cellulose, Ba(OH)$_2$, NiCl$_2$·6H$_2$O, HCl (37 wt%), OsO$_4$ (4 wt%), glutaraldehyde, and ethanol were purchased from Sigma Aldrich (St. Louis, MO, USA). Paraformaldehyde (8 wt%) was sourced from Thermo Fisher Scientific (MA, USA). Low-density polyethylene (LDPE, LB7500N, LG Chem, Republic of Korea) was kindly provided by Yonsei University. We utilized all chemicals in their analytical grade without further modification. Edible natural cuttlefish ink (*Sepia Officinalis*, from Stareef Seafood Boston, Product of Spain) was purchased in a Montreal fish market. For Sepia melanin extraction (see below), we used: HCl (ACS Reagent, 37 wt%, Acros Organics, Canada), monobasic sodium phosphate (0.2 M in H$_2$O), dibasic sodium phosphate solution (0.5 M in H$_2$O), ethanol (ACS reagent 99.8%), ethyl acetate, 1-propanol (≥ 99.5%), from Sigma Aldrich. ZrO$_2$ beads (1 mm Ø, density 5.5 g/cm^3) were purchased from Next Advance Inc. De-waxed shellac (AFS 701 Dewaxed Shellac) was received from AF Suter and Co. Ltd in the year 2021 and stored it in the refrigerator (4 °C) in the laboratory in order to preserve its quality.

Sepia melanin extraction, ink formulation, and printing

Extraction and purification of Sepia melanin powders from the raw ink of the cuttlefish are reported elsewhere[17]. Briefly, 300 g of cuttlefish ink was mixed with 500 mL of 2 M HCl and stirred for 24 hr at room temperature. We sequentially centrifuged (Allegra-X30R Centrifuge, Beckman Coulter) the slurry: first three times using 0.5 M HCl, followed by single centrifugation with de-ionized (DI) water, a single time with a buffer solution (composed of 0.02% v/v of 0.2 M monobasic sodium phosphate, 32.49% v/v of 0.2 M dibasic sodium phosphate and 67.49% v/v of DI water), a single time in ethanol and finally in ethyl acetate. For excess solvent removal, we rinsed, dispersed, and performed four centrifugations with DI water. We performed each centrifugation step at 10,000 rpm and 5 °C but varied the durations for each solvent. (15 min for 2 M HCl, 0.5 M HCl, ethanol, and ethyl acetate, 25 min for DI and the buffer solution). Finally, the powders were lyophilized for 3 d at -80 °C to remove excess water.

Sepia melanin-shellac ink was formulated as follows: first, 100 g of dewaxed shellac was dissolved in 242 g of 1-propanol. The blend was mixed in a high-rotation speed disperser (1.5 hp, Engineered Mills Inc.) at 500 rpm, for 3 hr. Afterward, 100 g of manually ground Sepia melanin powder was gradually added to the blend and mixed for 1 hr at 350 rpm. We transferred the ink to an attritor (high-rotation speed flat disc and 500 g of ZrO$_2$ beads), mixing it at 2000 rpm for 9 hr (total applied energy of about 1.2 kWh), to reduce the size of agglomerations in the ink and induce homogeneity. All mechanical stirring was performed in a water-cooled vessel at 10 °C. Sepia melanin powders, Sepia melanin shellac inks, and shellac were stored in a refrigerator (5 °C) in the dark.

Flexography is a roll-to-roll printing technique commonly used in the printing industry (e.g., newspapers, cardboards, and printed electronics) to transfer patterns of ink from a patterned plate onto a flexible substrate[48]. This technique was used for printing, utilizing a Flexiproof 100 laboratory flexographic printer (RK Printcoat Instruments, Canada). The process began with the deposition of ink onto an anilox roll, featuring cells measuring 15 × 10^9 cubic microns per square inch, using a doctor blade. This ink was then transferred first to the polymer printing plate and subsequently to the impression cylinder, which held the Kromekote® paper substrate. For clarity, Kromekote® paper, a paper coated with Kaolin (Al$_2$Si$_2$O$_5$(OH)$_4$), Ti, Mg, and Ca oxides[49], will henceforth be referred to simply as 'paper'. The end product, a Sepia melanin-shellac-printed film on silver-patterned paper, will be referred to as 'printed film'. [26]. For the thickness measurements, see Supplementary methods.

Dielectric spectroscopy

We performed dielectric spectroscopy measurements using a broadband dielectric/impedance spectrometer (Alpha-A High-Performance Frequency Analyzer, Novocontrol Technologies GmbH). The Shellac film was spin coated (0.1 g/mL in pure ethanol) at a maximum speed of 2500 rpm for 30 s on the glass slides bearing the gold (Au) electrodes and dried at 70 °C for 30 minutes in air. Aluminum is deposited to form the orthogonal crossing of the two pairs of metal electrodes 12 MIM (3×4 metal-insulator-metal) samples with similar thicknesses were fabricated for the dielectric measurements. We averaged the results across the 12 samples investigated. A typical measurement sweep involved 120 points of capacitance recordings of the MIM structure, from a start frequency of 10 kHz down to an end frequency of 1 mHz, over an applied AC voltage of 0.5 V. The top and bottom metals for the impedance measurements were aluminum and gold respectively, deposited in 80 nm-thick films by physical vapor deposition.

The breakdown field measurements were performed on the same instrument mentioned above for the impedance investigations, connected to a DC booster of ± 500 V. A typical measurement started at 0 V and comprised of a DC scan of a capacitance of the MIM structure with 2 V increment and 5 s hold time at each measurement point. The breakdown field was considered at the particular voltage where a sudden drop of the capacitance for at least two orders of magnitude occurred. The samples measured for the dielectric spectroscopy measurements were also subjected to breakdown field investigations. We fabricated samples of various thicknesses from about 400 nm to about 2000 nm, by spin coating at a fixed rotation speed of 2500 rpm from shellac solutions of different concentrations in ethanol.

Electrode fabrication

For fabricating silver electrodes on paper, we transferred silver water-based ink (PFI-500 Conductive Flexo Ink from Novacentrix) using a roll-to-roll press equipped with flexography printing units (OMET Varyflex V2)[50]. The interdigitated electrodes (25×2 fingers, 25 cm total channel length, 325 nm thick) have an interelectrode distance of 100 µm.

Electrical characterization

Current-voltage (I-V), transient current (I-t), and impedance spectroscopy (IS) characteristics were acquired in ambient (17 °C, 30% relative humidity, RH) and high humidity conditions using an Agilent B1500 semiconductor parameter analyzer. For measurements under controlled humidity, 85% RH was obtained in a Cole-Parmer Mini Humidity Chamber (model 03323−14) using a saturated salt solution of potassium sulfate (K_2SO_4, 2 g mL^{-1} in a 30 cm Ø glass container). A fan was used to ventilate and uniformly moisturize the chamber. We monitored the change in RH using two devices: a USB portable hygrometer (REED R6020 Datalogger) and an ETS microcontroller sensor (ETS 5100). Samples were left in the hydration chamber for at least 24 hr after which they were characterized in the same hydration chamber, in the same conditions. The weight gained after hydration was calculated by weighing the samples (printed films) before and after 24 hr-long hydration.

IS measurements were performed in the frequency range 3 mHz–3 MHz (20 points per decade, 10 mV oscillation) using a Biologic potentiostat (model VSP 300). IS data were fitted using Zview 4 software and fitting/simulation tools.

The electrical conductivity (σ) was calculated with the following equation:

$$\sigma = \frac{L}{R \times A}$$

With L, R, and A respectively the interelectrode distance (100 µm), the resistance extracted by Ohm's law or IS fit, and the cross-sectional area (channel width × thickness of the printed film, i.e., 25 cm × 5 µm).

Biodegradation test under composting conditions

Inoculum used in the biodegradation test was a three-month-old compost dedicated to the biodegradation of organic compounds (e.g., manure) (ABNEXO, Republic of Korea). The compost was comprised of 27.2% ash content, 36.4% volatile solids (VS), pH 8.6, and carbon/nitrogen ratio of 15:9. Before the biodegradation test, the compost was sieved using a 1.0 mm sieve to improve the homogeneity and prevent the inclusion of large particulate material such as sawdust. In each of the five types of bioreactors, we put 6 g (dry weight) of compost gently mixed with Sepia melanin powder, shellac flakes, printed films, α-cellulose powder, and LDPE sheets, respectively (see Table 1). The specific respiration rate of the reference compost was 10.5 ± 2.7 mg CO_2 g VS^{-1} d^{-1} for the initial 12 d.

To assess the respired CO_2, we employed a respirometer previously described in ref. 41. High-purity air (99.999%, Jeil Gas, Republic of Korea) was supplied to the respirometer throughout the test. Firstly, CO_2 in the air was eliminated by passing the air through 1 L of 0.025 M Ba(OH)$_2$ scrubbing solution. The air was then distributed into 15 channels using a regulator and a flowmeter and finally flushed in a DI water tank (maximum volume: 250 mL, working volume: 30–50 mL) to bring the moisture into the bioreactors. The CO_2-free and moisturized air was continuously supplied at 80–100 mL min^{-1}. The incubation was conducted in the dark at 58 °C and the water content of the compost was maintained between 50–60% (wt%) by regularly adding DI water, assuming that the weight loss of the bioreactors (i.e., compost, material, and glass bottle) was solely due to water evaporation from the compost. We manually mixed the compost biweekly. The CO_2 produced from each bioreactor was captured by passing through two consecutive stages of 200 mL of 0.025 M Ba(OH)$_2$ solutions and periodically titrated with 0.01 M HCl. Titration was performed every 2–3 d for the first 30 d, and less frequently in the following until 85 d of incubation (21 times in total) using an Orion Star T900 automatic titrator. Data are the average of triplicata. The averages of respired CO_2 from each bioreactor, net CO_2 produced (difference between the respired CO_2 (mg) of the sample and the respired CO_2 of the reference), and mineralization (%) were calculated, while the standard deviations were cumulatively computed. A detailed description of the calculations to obtain the biodegradation level (mineralization) is included in the Supporting Information (Supplementary Figs. 13–15, Supplementary Table 3)[26,28,30,51]. For the elemental analysis and calculation of the mineralization, see Supplementary methods. For the data analysis, see Supplementary note.

Microcosm experiment

The biodegradation behavior of the printed films was also assessed visually, by performing a microcosm experiment. The printed films (ca. 500 mg) were mixed with 50 g of compost in a 10 cm-side polypropylene (PP) cubic box equipped with a 0.2 µm-mesh air filter on the cover. The printed film was incubated in a climate chamber maintained at 60% RH and 58 °C for 20 d. The soil covering the printed film was carefully removed and the sample was recovered using a PP spatula and an air blower every day to observe its degradation behavior. A portion of the printed film was retrieved on 13 d of incubation to observe the colonization of the surface by compost microorganisms by SEM.

Scanning Electron Microscopy (SEM)

The morphology of the printed films was characterized with a Quattro Environmental SEM (ESEM, Thermofisher Scientific) at about 10 kV voltage in backscattered mode. Samples were observed in low-vacuum mode (200 Pa).

Microbial colonization of the compost microorganism on the surface of the printed film was observed by SEM (FEI Quanta 250 FEG (FEI, USA) at 3 kV). The printed films were immersed in a fixing solution containing 2.5% paraformaldehyde-glutaraldehyde buffered with 0.1 M phosphate buffer solution (pH 7.2) for 2 hr. Subsequently, the samples were washed for 10 min using the same buffer and fixed using the 1% wt% OsO$_4$ in 0.1 M phosphate buffer solution, at 25 °C, for 1 hr. The printed films were then dehydrated through a series of ethanol/isoamyl acetate solutions with

increasing concentrations (ethanol in isoamyl acetate 30%, 50%, 70%, 80%, 98%, and 100%) for 10 min each step and underwent critical point drying using liquid CO_2 with an EM CPD300 (Leica, Germany). Finally, gold was deposited on the surface of the printed films using a sputter coater SC502 (POLARON, Canada).

Microbial community analysis

The metagenome analysis was performed to investigate the microbial community involved in the biodegradation of Sepia melanin, shellac, printed films, and cellulose. On day 85 of the biodegradation test, 0.25 g of the compost samples were collected and analyzed through 16S rRNA gene amplicon sequencing. DNA extraction was performed using DNeasy PowerSoil Pro Kit (Qiagen, Hilden, Germany), following the protocol provided by the manufacturer. The V3–V4 region of the 16s rRNA gene was amplified using a 341F–805 R primer set, and the sequencing of the generated amplicons was conducted by Macrogen Inc. (Seoul, Republic of Korea) on the Miseq platform (Illumina, CA, USA). The raw paired-end amplicon sequence data were analyzed using the QIIME2 v2022.8 pipeline. The reads were clustered into amplicon sequence variants (ASVs) using the DADA2 plugin. Unique ASVs were taxonomically assigned using a scikit-learn Naive Bayes classifier pre-trained with Silva SSU Ref NR 99 database 138[52]. Raw sequencing data are available at the Sequence Read Archive (SRA) of the National Center for Biotechnology Information (NCBI) under BioProject accession number PRJNA1019117.

Phytotoxicity test

The potential terrestrial phytotoxicity of the biodegradation byproducts (i.e., residual material) on plant germination was investigated in accordance with OECD 208[42,53]. A commercially available loamy soil (composed of coke peat, peat moss, perlite, zeolite, clay sand, humus, and fermented bark, Biophilia Co., Republic of Korea) characterized by a water holding capacity of 50.2% and pH 6.4–6.8 was used as substratum. After the biodegradation test, 2.2 g of compost was retrieved from each vessel and mixed with 11.0 g of soil. Subsequently, twenty seeds of ryegrass (*Lolium multiflorum*) were sown in a 9 cm-∅ Petri dish containing compost and soil mixture. Petri dishes were covered with cylindrical poly(ethylene terephthalate) cups (135 mm-∅), where 5 holes had been pierced. The Petri dishes contained 2.2 g of reference compost (i.e., compost used as reference in biodegradation test), compost + Sepia melanin, compost + shellac, compost + printed film, compost + cellulose, compost + LDPE (biodegradation products only: the LDPE sheets was removed), reference compost + $NiCl_2$ (1 and 5 wt%, denoted as $NiCl_2$-1 and $NiCl_2$—5) and soil, respectively. $NiCl_2$ was used as phytotoxic positive control[54].

The test was performed in controlled light, humidity, and temperature conditions via a plant incubation chamber Tiiun (LG Electronics, Republic of Korea). Planted seeds were incubated in the dark for the first 2 d, then exposed to a diurnal photoperiod cycle: dark for 8 hr and light for 16 hr at $20.8 \pm 3.2\,°C$ and $49.4 \pm 13.7\%$ RH, with light intensity of 5500 ± 500 lux. The temperature and humidity conditions were monitored using a data logger RC-4HC (Elitech, CA, USA, Supplementary Fig. 16). DI water was automatically supplemented in the incubator from the water tank in the incubation chamber (Tiiun). After 14 d of incubation, the germinated plants were collected, and seedling emergence, shoot wet mass, and shoot length were measured. Shoots were cut at the soil line, and fresh biomass was immediately determined.

The effect of the printed films on plant growth was further examined with a commercial plant seed kit module (LG Electronics, Republic of Korea). Each kit contains five holes with sponges for harboring plant tree seeds. A hundred milligrams of compost that contained printed films were retrieved at the end of the biodegradation test and placed within the kit holes. Marigold (*Tagetes erecta*) was cultured in the same incubator. Seedling emergence and plant phenotypes were visually assessed. No additional nutrients were provided to plants.

Statistics

The results are presented as mean ± standard deviation (SD). Student's *t*-test was conducted to determine the significant difference between the means of the two groups (reference vs samples, in phytotoxicity tests). The non-linear regression of the mineralization curves was carried out with Origin 2019. R (version 4.2.2) via R studio interface (v. 2023.06.2 + 561) was used for plotting principal coordinate analysis (PCoA) with *ape* package (version 5.7.1) and *ggplot2* (version 3.4.3) on a weighted UniFrac to compare beta diversity of microbial communities based on the phylogenetic relationships[55].

Data availability

Data is fully available upon request.

References

1. Forti, V., Balde, C. P., Kuehr, R. & Bel, G. The Global E-Waste Monitor 2020: Quantities, Flows and the Circular Economy Potential. *United Nations University/United Nations Institute for Training and Research, International Telecommunication Union, and International Solid Waste Association* (2020).
2. Ordoñez Duran, J. F., Chimenos, J. M., Segarra, M., de Antonio Boada, P. A. & Ferreira, J. C. E. Analysis of embodied energy and product lifespan: the potential embodied power sustainability indicator. *Clean. Technol. Environ. Policy* **22**, 1055–1068 (2020).
3. Meredith, P. & Sarna, T. The physical and chemical properties of eumelanin. *Pigment Cell Res.* **19**, 572–594 (2006).
4. Magarelli, M., Passamonti, P. & Renieri, C. Purification, characterization and analysis of sepia melanin from commercial sepia ink (Sepia Officinalis). *CES Medicina Veterinaria y. Zootecnia* **5**, 18–28 (2010).
5. Cheng, J., Moss, S. C. & Eisner, M. X-Ray Characterization of Melanins—I. *Pigment Cell Res.* **7**, 263–273 (1994).
6. Cheng, J., Moss, S. C. & Eisner, M. X-Ray Characterization of Melanins—II. *Pigment Cell Res.* **7**, 263–273 (1994).
7. Pezzella, A., D'Ischia, M., Napolitano, A., Palumbo, A. & Prota, G. An integrated approach to the structure of sepia melanin. Evidence for a high proportion of degraded 5,6-Dihydroxyindole-2-carboxylic acid units in the pigment backbone. *Tetrahedron* **53**, 8281–8286 (1997).
8. Thakuria, R., Nath, N. K. & Saha, B. K. The Nature and Applications of π-π Interactions: A Perspective. *Cryst. Growth Des.* **19**, 523–528 (2019).
9. Chen, T., Li, M. & Liu, J. π–π Stacking Interaction: A Nondestructive and Facile Means in Material Engineering for Bioapplications. *Cryst. Growth Des.* **18**, 2765–2783 (2018).
10. Hunter, C. A. & Sanders, J. K. M. The Nature of π-π Interactions. *J. Am. Chem. Soc.* **112**, 5525–5534 (1990).
11. Niyonkuru, D. et al. A nanoscale study of the structure and electrical response of Sepia eumelanin. *Nanoscale Adv.* **5**, 5295-5300 (2023).
12. Reali, M. et al. Electronic Transport in the Biopigment Sepia Melanin. *ACS Appl Bio Mater.* **3**, 5244–5252 (2020).
13. Mcginness, J., Corry, P. & Proctor, P. Amorphous semiconductor switching in melanins. *Science* **183**, 853–855 (1974).
14. Bernardus Mostert, A., Powell, B. J., Gentle, I. R. & Meredith, P. On the origin of electrical conductivity in the bio-electronic material melanin. *Appl Phys. Lett.* **100**, 1–3 (2012).
15. Bernardus Mostert, A. et al. Gaseous adsorption in melanins: Hydrophilic biomacromolecules with high electrical conductivities. *Langmuir* **26**, 412–416 (2010).
16. Mostert, A. B. et al. Role of semiconductivity and ion transport in the electrical conduction of melanin. *Proc. Natl Acad. Sci.* **109**, 8943–8947 (2012).

17. Camus, A. et al. High conductivity Sepia melanin ink films for environmentally benign printed electronics. *Proc. Natl Acad. Sci.* **119**, 1–8 (2022).

18. Nosanchuk, J. D. & Casadevall, A. The contribution of melanin to microbial pathogenesis. *Cell Microbiol.* **5**, 203–223 (2003).

19. Jacobson, E. S. Pathogenic roles for fungal melanins. *Clin. Microbiol Rev.* **13**, 708–717 (2000).

20. Thombare, N. et al. Shellac as a multifunctional biopolymer: A review on properties, applications and future potential. *Int J. Biol. Macromol.* **215**, 203–223 (2022).

21. Yuan, Y. et al. Shellac: A promising natural polymer in the food industry. *Trends Food Sci. Technol.* **109**, 139–153 (2021).

22. Irimia-Vladu, M. et al. Natural resin shellac as a substrate and a dielectric layer for organic field-effect transistors. *Green. Chem.* **15**, 1473–1476 (2013).

23. Irimia-Vladu, M. et al. Environmentally sustainable organic field effect transistors. *Org. Electron* **11**, 1974–1990 (2010).

24. Poulin, A., Aeby, X., Siqueira, G. & Nyström, G. Versatile carbon-loaded shellac ink for disposable printed electronics. *Sci. Rep.* **11**, 1–9 (2021).

25. Erdal, N. B. & Hakkarainen, M. Degradation of Cellulose Derivatives in Laboratory, Man-Made, and Natural Environments. *Biomacromolecules* **23**, 2713–2729 (2022).

26. Haider, T. P., Völker, C., Kramm, J., Landfester, K. & Wurm, F. R. Plastics of the Future? The Impact of Biodegradable Polymers on the Environment and on Society. *Angew. Chem. - Int. Ed.* **58**, 50–62 (2019).

27. Chandna, P., Nain, L., Singh, S. & Kuhad, R. C. Assessment of bacterial diversity during composting of agricultural byproducts. *BMC Microbiol*. **13**, 99 (2013).

28. Choe, S., Kim, Y., Won, Y. & Myung, J. Bridging Three Gaps in Biodegradable Plastics: Misconceptions and Truths About Biodegradation. *Front Chem.* **9**, 1–8 (2021).

29. Nelson, T. F. et al. Biodegradation of poly(butylene succinate) in soil laboratory incubations assessed by stable carbon isotope labelling. *Nat. Commun.* **13**, 1–16 (2022).

30. Zumstein, M. T. et al. Biodegradation of synthetic polymers in soils: Tracking carbon into CO_2 and microbial biomass. *Sci. Adv.* **4**, eaas9024 (2018).

31. Sander, M. Biodegradation of Polymeric Mulch Films in Agricultural Soils: Concepts, Knowledge Gaps, and Future Research Directions. *Environ. Sci. Technol.* **53**, 2304–2315 (2019).

32. Egginger, M. et al. Mobile ionic impurities in poly (vinyl alcohol) gate dielectric: Possible source of the hysteresis in organic field-effect transistors. *Adv. Mater.* **20**, 1018–1022 (2008).

33. Coppola, M. E. et al. Pinaceae Pine Resins (Black Pine, Shore Pine, Rosin, and Baltic Amber) as Natural Dielectrics for Low Operating Voltage, Hysteresis-Free, Organic Field Effect Transistors. *Glob. Chall.* **7**, 2300062 (2023).

34. D'Orsi, R. et al. Kraft Lignin: From Pulping Waste to Bio-Based Dielectric Polymer for Organic Field-Effect Transistors. *Adv. Sustain Syst.* **6**, (2022).

35. Zhao, L. & Liu, C. L. Review and mechanism of the thickness effect of solid dielectrics. *Nanomaterials* **10**, 1–24 (2020).

36. Huggins, R. A. Simple method to determine electronic and ionic components of the conductivity in mixed conductors a review. *Ion.* **8**, 300–313 (2002).

37. Sheliakina, M., Mostert, A. B. & Meredith, P. Decoupling Ionic and Electronic Currents in Melanin. *Adv. Funct. Mater.* **28**, 1–7 (2018).

38. Schlingman, K., Chen, Y., Carmichael, R. S. & Carmichael, T. B. 25 Years of Light-Emitting Electrochemical Cells: A Flexible and Stretchable Perspective. *Adv. Mater.* **33**, 1–20 (2021).

39. García-Batlle, M. et al. Coupling between Ion Drift and Kinetics of Electronic Current Transients in MAPbBr3 Single Crystals. *ACS Energy Lett.* **7**, 946–951 (2022).

40. Sharma, S. K., Shukla, S. K. & Vaid, D. N. SHELLAC - STRUCTURE, CHARACTERISTICS & MODIFICATION. *Def. Sci. J.* **33**, 261–271 (1983).

41. Choe, S. et al. Biodegradation of 3D-Printed Biodegradable/Non-biodegradable Plastic Blends. *ACS Appl Polym. Mater.* **4**, 5077–5090 (2022).

42. Di Mauro, E., Rho, D. & Santato, C. Biodegradation of bio-sourced and synthetic organic electronic materials towards green organic electronics. *Nat. Commun.* **12**, 1–10 (2021).

43. Ghoshal, S., Khan, M. A., Khan, R. A., Gul-E-Noor, F. & Chowdhury, A. M. S. Study on the Thermo-Mechanical and Biodegradable Properties of Shellac Films Grafted with Acrylic Monomers by Gamma Radiation. *J. Polym. Environ.* **18**, 216–223 (2010).

44. Purahong, W. et al. Back to the Future: Decomposability of a Biobased and Biodegradable Plastic in Field Soil Environments and Its Microbiome under Ambient and Future Climates. *Environ. Sci. Technol.* **55**, 12337–12351 (2021).

45. Wang, Y., Tang, Y. & Yuan, Z. Improving food waste composting efficiency with mature compost addition. *Bioresour. Technol.* **349**, 126830 (2022).

46. Zhang, Y. et al. Impact of Petroleum Contamination on the Structure of Saline Soil Bacterial Communities. *Curr. Microbiol*. **79**, 1–12 (2022).

47. Gao, Y. et al. Enhanced degradation of quinoline by coupling microbial electrolysis cell with anaerobic digestion simultaneous. *Bioresour. Technol.* **306**, 123077 (2020).

48. Blayo, A. & Pineaux, B. Printing processes and their potential for RFID printing. *ACM Int. Conf. Proc. Ser.* **121**, 27–30 (2005).

49. Bundy, W. M. & Ishley, J. N. Kaolin in paper filling and coating. *Appl Clay Sci.* **5**, 397–420 (1991).

50. Zhuldybina, M., Ropagnol, X., Bois, C., Zednik, R. J. & Blanchard, F. Printing accuracy tracking with 2D optical microscopy and super-resolution metamaterial-assisted 1D terahertz spectroscopy. *npj Flexible. Electronics* **4**, 1–7 (2020).

51. Ruggero, F., Gori, R. & Lubello, C. Methodologies to assess biodegradation of bioplastics during aerobic composting and anaerobic digestion: A review. *Waste Manag. Res.* **37**, 959–975 (2019).

52. Bolyen, E. et al. Reproducible, interactive, scalable and extensible microbiome data science using QIIME 2. *Nat. Biotechnol.* **37**, 852–857 (2019).

53. OECD. OECD Test Guideline 208: Terrestrial Plant Test - Seedling Emergence and Seedling Growth Test. *Guidelines for the Testing of Chemicals, Terrestrial Plant Test Seedling Emergence and Seedling Growth Test* **227**, 1–21 (2006).

54. Kumar, S. et al. Nickel toxicity alters growth patterns and induces oxidative stress response in sweetpotato. *Front Plant Sci.* **13**, 1–17 (2022).

55. Chang, Q., Luan, Y. & Sun, F. Variance adjusted weighted UniFrac: a powerful beta diversity measure for comparing communities based on phylogeny. *BMC Bioinforma.* **12**, 118 (2011).

Acknowledgements

Author contributions

Anthony Camus: Conceptualization, Methodology, Investigation, Data Curation, Writing - Original Draft, Writing - Review & Editing, Visualization; Shinhyeong Choe: Conceptualization, Methodology, Software, Investigation, Data Curation, Writing - Original Draft, Writing - Review & Editing, Visualization; Camille Bour-Cardinal: Investigation, Data Curation, Writing - Original Draft, Writing - Review & Editing, Visualization; Joaquin Isasmendi: Investigation, Data Curation, Writing - Review & Editing; Yongjun Cho: Methodology, Investigation, Writing - Review & Editing; Youngju Kim: Methodology, Investigation, Data Curation, Writing - Review & Editing; Cristian Vlad Irimia: Investigation, Data Curation; Cigdem Yumusak: Investigation, Data Curation; Mihai Irimia-Vladu: Investigation, Data Curation, Review & Editing, Visualization; Denis Rho: Data Curation, Writing - Original Draft, Writing - Review & Editing, Visualization; Supervision. Jaewook Myung: Conceptualization; Writing - Original Draft, Writing - Review & Editing, Supervision, Funding acquisition. Clara Santato: Conceptualization, Methodology, Writing - Original Draft, Writing - Review & Editing, Supervision, Funding acquisition.

Competing interests

The authors declare no competing interests

Additional information

Supplementary information The online version contains supplementary material available at https://doi.org/10.1038/s43246-024-00592-3.

Correspondence and requests for materials should be addressed to Denis Rho, Jaewook Myung or Clara Santato.

Peer review information *Communications Materials* thanks Robin Bonne and the other, anonymous, reviewer(s) for their contribution to the peer review of this work. Primary Handling Editors: Rona Chandrawati and John Plummer.

Reprints and permissions information is available at http://www.nature.com/reprints

Publisher's note Springer Nature remains neutral with regard to jurisdictional claims in published maps and institutional affiliations.